Article ID: 1000-324X(2015)12-1334-05 **DOI:** 10.15541/jim20150245

Fabrication of Barium Strontium Titanate Nanophotocatalysts with Gridding Structures and Their Photocatalytic Activities

ZENG Tao[1], BAI Yang[1], LI Hao[2], MAO Chao-Liang[3], DONG Xian-Lin[3], GUI Shu-Xiang[1]

(1. Shanghai Key Laboratory of Materials Protection and Advanced Materials in Electric Power, Shanghai University of Electric Power, Shanghai 200090, China; 2. Department of Chemical Engineering, Huizhou University, Huizhou 516007, China; 3. Key Laboratory of Inorganic Functional Materials and Devices, Shanghai Institute of Ceramics, Chinese Academy of Sciences, Shanghai 200050, China)

Abstract: $Ba_{0.7}Sr_{0.3}TiO_3$ (BST) nanocatalysts were prepared by a Sol-Gel method at pH of 2.4 and 4, respectively, both of which were presented as tetragonal phase. TEM images indicated that the BST sample obtained at pH = 2.4 was nanoparticles with an average size of about 100 nm, while that obtained at pH = 4 was gridding structures composed of nanocubes with a mean size of 100 nm. The photocatalytic behavior of BST in the degradation of Rhodamine B (RhB) was investigated. It was found that the BST catalysts with gridding structures showed much better photocatalytic performance than the BST nanoparticles. This could be attributed to the fact that the photo-generated carriers can migrate easily through the gridding-structured BST sample, which would enhance the photocatalytic activity during the degradation process. It was also found that both BST photocatalysts in this work showed good catalytic stability.

Key words: (Ba, Sr)TiO_3; gridding-structure; photocatalyst; Sol-Gel

Pollution caused by organic pollutants is a serious problem for environmental protection. During the past decades, many techniques, such as membrane bioreactors[1], activated sludge treatments[2-3], advanced oxidation processes[4-6], have been developed for the degradation of organics in wastewaters or in air. Owing to its low cost, nontoxicity, easy operation, effective and environmentally friendly properties, the catalytic oxidation method, especially the photocatalytic oxidation method is regarded as the most promising method for pollution control.

During photocatalysis process, photocatalyst particles suspended in organic-containing wastewater are irradiated with light. The oxidative species generated on the surface of photocatalysts will react with organic contaminants and thus result in the degradation of organic pollutions[7]. Hence, the selection of photocatalysts is critical, which determines the overall efficiency of the photocatalytic degradation of organics. Among all photocatalysts, semiconductor based photocatalysts have been extensively investigated due to their narrow band gap, which can absorb a large fraction of visible light in solar radiation. However, there are still some problems which limit their practical applications[8]. For example, a high rate of electron-hole recombination on photocatalyst surface reduces the efficiency of photocatalysis. Even though the heterostructured photocatalysts were developed to reduce the recombination rate of electron-hole by separation of the electron and hole in two kinds of semiconductors respectively, the existence of the second inactive semiconductor may decrease the catalytic efficiency.

One route to solve these problems is to develop new types of photocatalytic materials. Steven's group firstly proposed the utilization of the spontaneous polarization in ferroelectrics to separate the electrons and holes[8]. In that case, instead of heterostructure photocatalysts, a ferroelectric photocatalyst can be used to decrease the recombination rate of electron-hole. This may open up a new approach to enhance the photocatalytic activity.

However, there are only a few literatures on ferroelectrics for photocatalysis applications. In addition, compared with semiconductor photocatalysts, ferroelectrics generally have relatively lower photocatalytic activity. So it is important to develop other photocatalysts of ferroelectrics with high photocatalytic activity for its further application as photocatalysis. BST ($Ba_{1-x}Sr_xTiO_3$, $0<x<1$) is a typical ferroelectrics with large remnant polarization[9-10], which receives much attentions for its high dielectric, ferroelectric and pyroelectric properties. However, the photocata-

Received date: 2015-05-22; **Modified date:** 2015-08-31; **Published online:** 2015-09-30
Foundation item: Science and Technology Commission of Shanghai Municipality (14DZ2261000); High-level Talent Project of the University in Guangdong Province
Biography: ZENG Tao(1977-), male, associate professor. E-mail: zengtao@shiep.edu.cn

lytic behaviors of BST are seldom concerned.

In this work, the photocatalytic behaviors of BST prepared by a Sol-Gel method were investigated. By adjusting the pH values of the reaction media, BST nanoparticles and gridding structure composed of nanocubes were obtained. The catalytic degradation of Rhodamine B was applied as a probe reaction to test the catalytic performance of the photocatalysts. It was found that the BST with gridding-structure exhibited better catalytic properties that the nanoparticels.

1 Experimental

1.1 Materials and synthesis

$Ba(CH_3COO)_2$, $Sr(CH_3COO)_2$ and $Ti(C_4H_9O)_4$ were used as starting materials to synthesize $Ba_{0.70}Sr_{0.30}TiO_3$ (BST) powders. Acetic acid and ethanol were applied as solvents for the acetates and alkoxide, respectively. Acetylacetone was used as an additive to stabilize the solution. All the reagents were of analytical grade and used without further purification. First, 7 mmol $Ba(CH_3COO)_2$ and 3 mmol $Sr(CH_3COO)_2$ were dissolved into 80 mL Acetic acid together with stirring vigorously, and 10 mmol $Ti(C_4H_9O)_4$ was mixed with 30 mL ethanol. Then the two individual solutions were thoroughly mixed to form a transparent solution. Acetylacetone (2 mol) per titanium ion was then added to the transparent solution. After that, $NH_3{\cdot}H_2O$ (5wt%) was added to adjust the pH of the solution to 2.4 and 4, respectively. After stirring for 10 h, an orange sol was obtained. Then the sol was dried at 120℃ for 12 h to obtain xerogel. The xerogel was grinded into powers and used as precursor. Then the BST was obtained after calcining the precursor at 900℃ for 8 h.

1.2 characterizations

X-ray diffraction (XRD) was performed on a Bruker D8 Advance diffractometer using Cu Kα radiation. UV-visible diffuse reflectance spectra (UV-DRS) of the samples were obtained on an UV-visible spectrophotometer (UV-2550, Shimadzu) and the absorption spectra was obtained by standard Kubelka-Munk method. Transmission electron microscopy (TEM) images were observed by a JEM-2100F transmission electron microscope. The specific surface areas of the samples were deduced according to the Brunauer-Emmett-Teller (BET) method using a Gemini VII 2390 surface area analyzer.

1.3 photocatalytic experiments

The photocatalytic experiment was carried out as following: A 300 W Xe lamp was used as the light source. 0.5 g photocatalyst was added into 100 mL of 20 mg/L RhB solution. Prior to illumination, the suspension was vigorously stirred in the dark for 1 h to ensure an adsorption/desorption equilibrium for RhB solution and photocatalyst. Then the suspension was exposed to light irradiation. UV-visible spectrophotometer was used to monitor the concentration of RhB by measuring the absorbance at 552 nm. And a dialyzer was used to remove the photocatalyst in the suspension withdrawed every certain interval.

2 Results and Discussion

The crystal phases of the as-prepared $Ba_{0.7}Sr_{0.3}TiO_3$ were investigated with XRD (Fig. 1). It can be seen that both the BST samples prepared at pH of 4 and 2.4 are well crystallized. All the diffraction peaks can be well indexed to the tetragonal BST (ICSD 44-0093). No other characteristic peaks were found. The intensities of the peaks in the XRD pattern of BST sample obtained at pH = 4 is higher than those obtained at pH = 2.4, indicating that the sample obtained at pH = 4 possesses higher degree of crystallinity.

The morphologies and microstructures of the samples were investigated with TEM. As shown in Fig. 2, most of

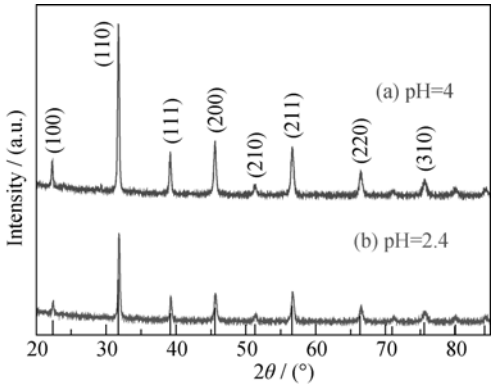

Fig. 1 XRD patterns of the BST at different pH

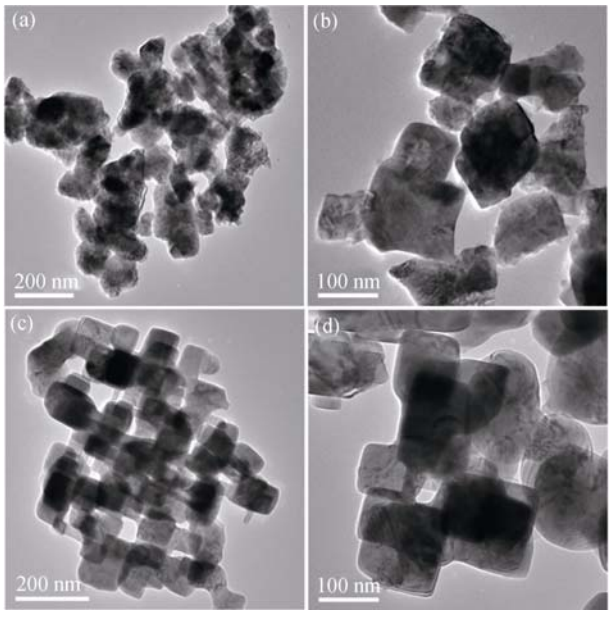

Fig. 2 TEM images of the (a, b) BST (pH=2.4) and (c, d) BST (pH=4)

the particles obtained at pH = 2.4 were square-like. The average particle diameter was about 100 nm. It could be also seen from Fig. 2(a) and Fig. 2(c) that BST sample synthesized at pH = 4 was more homogenously square compared with that synthesized at pH value of 2.4, which also demonstrate higher crystallinity of BST synthesized at pH value of 4. Another interesting phenomenon is that a kind of gridding-structures composed of many nanocubes began to form when the pH value reached 4. The formation of this structure could be attributed to the enhanced chelation with increasing pH value, which led to the homogenous distributions of metal ions in the gel.

The hydrolysis reaction of $Ti(C_4H_9O)_4$ leads to the formation of $Ti(OH)_x(OC_4H_9)_{4-x}$. This is probably owing to the fact that when the pH of the medium was lower, the quantity of the hydroxyl groups in it was smaller, which limited the hydrolysis of alkoxide. And the higher the pH was, the bigger the value of x, resulting in sufficiently hydrolysis. On the other hand, when the pH increased, the chelation of metal ion and acetate was enhanced, leading to better homogeneity and better crystallization in the followed process[11-12]. During the annealing process, when large amounts of butoxy group and acetate ion in the xerogel were removed, gaps formed between nanoparticles[13-14]. Thus, the gridding-structured composed of tetragonal BST nanoparticles were obtained. The schematic illustration of possible formation mechanism for gridding-structured BST is shown in Fig. 3.

As the ordering of a nanocrystalline structure considerably generates big influence on the charge transport and recombination, which are directly related to the performance of photocatalysts[15-17], the gridding-structured BST synthesized at pH of 4 are expected to exhibit better performance of photocatalysis. As shown in Fig. 3e, the superstructure facilitated the charge separation and the charges were remarkably long-lived. Thereby, the photocatalytic activities were greatly enhanced.

The optical absorption of the BST samples, which is a key factor in determining photocatalytic behavior, was measured by UV-Vis spectrometer. Figure 4 shows the typical diffuse reflection spectrum of the two samples. The steep shape of the spectrum demonstrated that the UV-light absorption was due to the band gap transition, not due to the transition from impurity level[18]. It can be seen from Fig. 4 that the spectrum of BST (pH=2.4) sample is similar to that of the BST (pH=4) sample. And the value of band gap of the two samples were estimated to 3.2 eV accoding to the equation E_g=1240/λ_g eV, where E_g, λ_g are band gap and absorption wavelength threshold, respectively. This could be ascribed to the fact that the two BST catalysts have the same crystal structures.

The photocatalytic activities of the samples are evaluated by using the Rhodamine B as the decomposed target molecules in an aqueous solution under visible light irradiation. The blank test indicated that the degradation was very slow without photocatalyst under visible light illumination. The degradation efficiency reached 91% within 80 min by photocatalyst BST (pH=4). But the degradation efficiencyby BST (pH=2.4) is only about 75% in 80 min. According to the apparent pseudo-first-order kinetics equation, the degradation rate constant was estimated *via* the formula

$$\ln(C/C_0) = -kt$$

In this formula, k is the apparent first order reaction rate constant of RhB degradation. The value of k was obtained by calculating the slope of lines in Fig. 5(b) and the results are listed in Table 1. The rate constants of RhB degradation catalyzed by BST (pH=2.4) and BST (pH=4) are 0.018 min^{-1} and 0.059 min^{-1}, respectively. The higher phtocatalytic efficiency of BST (pH=4) may be attributed to the special gridding-structure, higher specific surface areas and better crystallinity. The gridding-structured is beneficial in that the photogenerated e^- was allowed to migrate between adjacent BST nanocrystals[13] and thus, recombination of photogenerated electrons (e^-) and holes (h^+) in both the bulk and on the surface was inhibited.

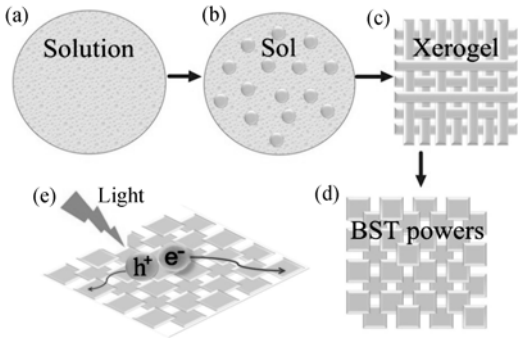

Fig. 3 Schematic illustration of the formation process for BST gridding-structure (a-d) and the separation process for photogenerated carries (e)

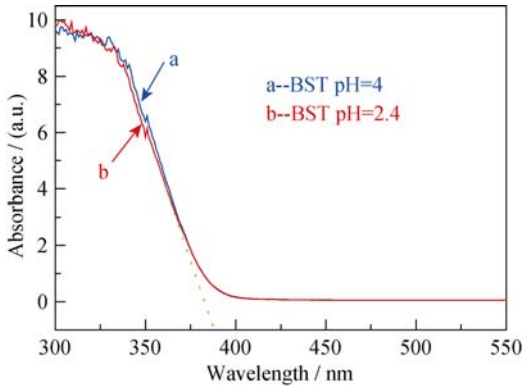

Fig. 4 Typical diffuse reflection spectrum of the BST

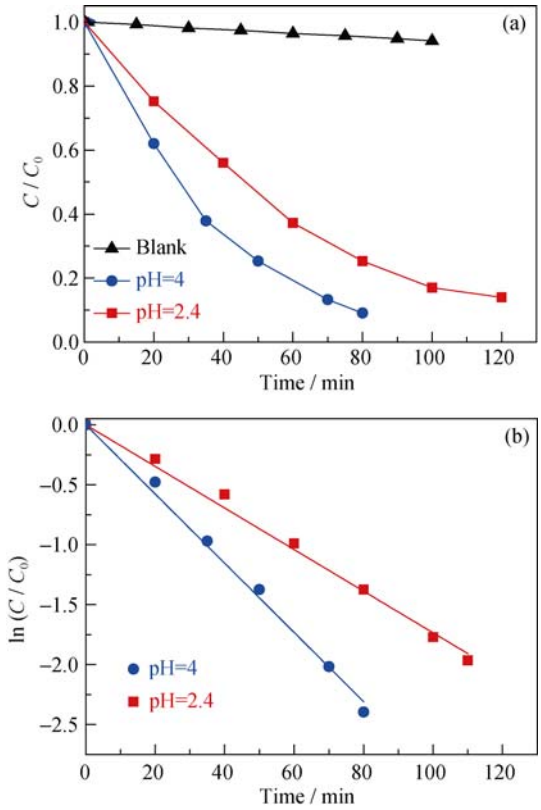

Fig. 5 Normalized concentration of RhB (a) and logarithm of normalized concentration of RhB (b) at different reaction time

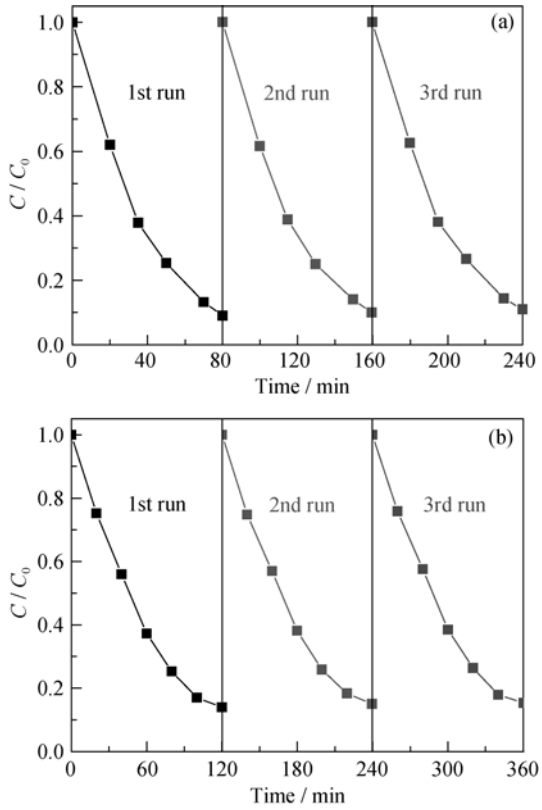

Fig. 6 Cycling runs in the photocatalytic degradation of RhB in the presence of BST (pH=4) (a) and BST (pH=2.4) (b)

Table 1 The BET surface areas of the different BST catalysts, the rate constants in the degradation of RhB

Sample	BST (pH=2.4)	BST (pH=4)
BET surface/($m^2 \cdot g^{-1}$)	6.12	7.87
Rate constant/min^{-1}	0.018	0.059

For its application, the stability of a photocatalyst is very important. As shown in Fig. 6, after three catalytic recycles for the photodegradation of RhB, both of the photocatalysts did not show obvious activity loss. These facts indicated that the BST had excellent stability and photo-corrode resistance after three cycles of degradation.

3 Conclusions

BST ($Ba_{0.7}Sr_{0.3}TiO_3$) powders were prepared by Sol-Gel method in different pH values. The photocatalytic behavior of BST in the degradation of Rhodamine B (RhB) was investigated. The better photocatalytic performance for BST catalyst fabricated at the pH value of 4 can be attributed to its gridding-structure. In this structure, nano square BST grains connect with each other, so the photo-generated carriers can be easy to move through the BST grains, which enhance the photocatalytic activity during the degradation process. Both of the BST photocatalysts showed good catalytic stability after three cycles of degradation.

References:

[1] PIERRE LE-CLECH, CHEN VICKI, FANE TONY A G. Fouling in membrane bioreactors used in wastewater treatment. *J. Membrane. Sci.*, 2006, **284(1/2):** 17–53.

[2] ZÜMRIYE AKSU. Biosorption of reactive dyes by dried activated sludge: equilibrium and kinetic modeling. *Biochem. Eng. J.*, 2001, **7(1):** 79–84.

[3] ELISABETH NEYENS, JAN BAEYENS, RAF DEWIL, *et al*. Advanced sludge treatment affects extracellular polymeric substances to improve activated sludge dewatering. *J. Hazard. Mater.*, 2004, **106(2/3):** 83–92.

[4] ROBERTO ANDREOZZI, VINCENZO CAPRIO, AMEDEO INSOLA, *et al*. Advanced oxidation processes (AOP) for water purification and recovery. *Catalysis Today*, 1999, **53(1):** 51–59.

[5] BIAN ZHEN-FENG, TAKASHI TACHIKAWA, ZHANG PENG, *et al*. Au/TiO_2 superstructure-based plasmonic photocatalysts exhibiting efficient charge separation and unprecedented activity. *J. Am. Chem. Soc.*, 2014, **136(1):** 458−465.

[6] NEYENS E, BAEYENS J. A review of classic Fenton's peroxidation as an advanced oxidation technique. *J. Hazard. Mater.*, 2003, **98(1/2/3):** 33–50.

[7] YANG XIAO-FEI, CUI HAI-YING, LI YANG, *et al*. Fabrication

of Ag_3PO_4-graphene composites with highly efficient and stable visible light photocatalytic performance. *ACS Catal.*, 2013, **3(3):** 363−369.

[8] MATT STOCK, STEVE DUNN. Influence of the ferroelectric nature of lithium niobate to drive photocatalytic dye decolorization under artificial solar light. *J. Phys. Chem. C*, 2012, **116(39):** 20854−20859.

[9] WANG JIANG-YING, YAO XI, ZHANG LIANG-YING. Preparation and dielectric properties of barium strontium titanate glass-ceramics sintered from Sol–Gel-derived powders. *Ceram. Int.*, 2004, **30(7):** 1749–1752.

[10] JANG H M, JUN Y H. (Ba, Sr)TiO_3 system under dc-bias field. II: Induced and intrinsic pyroelectric coefficients and figures-of-merit. *Ferroelectrics*, 1997, **193(1):** 125–140.

[11] LIU JUN-LIANG, ZHANG WEI, GUO CUIJING, *et al*. Synthesis and magnetic properties of quasi-single domain M-type barium hexaferrite powders *via* Sol–Gel auto-combustion: effects of pH and the ratio of citric acid to metal ions (CA/M). *J. Alloys Compd.*, 2009, **479(1/2):** 863–869.

[12] YU JIA-GUO, SU YAO-RONG, CHENG BEI, *et al*. Effects of pH on the microstructures and photocatalytic activity of mesoporous nanocrystalline titania powders prepared *via* hydrothermal method. *J. Mol. Catal. A-Chem.*, 2006, **258(1/2):** 104–112.

[13] BIAN ZHEN-FENG, TAKASHI TACHIKAWA, TETSURO MAJIMA. Superstructure of TiO_2 crystalline nanoparticles yields effective conduction pathways for photogenerated charges. *J. Phys. Chem. Lett.*, 2012, **3(11):** 1422−1427.

[14] BIAN ZHEN-FENG, TAKASHI TACHIKAWA, KIM WOOYUL, *et al*. Superior electron transport and photocatalytic abilities of metal nanoparticle- loaded TiO_2 superstructures. *J. Phys. Chem. C*, 2012, **116(48):** 25444−25453.

[15] LAKSHMINARASIMHAN N, KIM W, CHOI W. Effect of the agglomerated state on the photocatalytic hydrogen production with *in situ* agglomeration of colloidal TiO_2 nanoparticles. *J. Phys. Chem. C*, 2008, **112(51):** 20451−20457.

[16] ISMAIL A A, BAHNEMANN D W. Mesostructured Pt/TiO_2 nanocomposites as highly active photocatalysts for the photooxidation of dichloroacetic acid. *J. Phys. Chem. C*, 2011, **115(13):** 5784−5791.

[17] GONZALEZ-VAZQUEZ J P, MORALES-FLÓ REZ V, ANTA J A. How important is working with an ordered electrode to improve the charge collection efficiency in nanostructured solar cells? *J. Phys. Chem. Lett.*, 2012, **3(3):** 386−393.

[18] KUDO A, TSUJI I, KATO H. $AgInZn_7S_9$ solid solution photocatalyst for H_2 evolution from aqueous solutions under visible light irradiation. *Chem. Commun.*, 2002, **17:** 1958–1959.

纳米网状结构钛酸锶钡的制备及其催化性能研究

曾 涛[1], 白 杨[1], 李 浩[2], 毛朝梁[3], 董显林[3], 桂书祥[1]

(1. 上海电力学院 上海市电力材料防护与新材料重点实验室, 上海 200090; 2. 惠州学院 化学工程系, 惠州 516007; 3. 中国科学院 上海硅酸盐研究所, 无机功能材料与器件重点实验室, 上海 200050)

摘 要: 采用溶胶–凝胶法在不同 pH 值条件下制备了纳米钛酸锶钡(BST)粉体。在 pH 值为 4 和 2.4 条件下合成的 BST 粉体都是单相并结晶良好。透射电镜结果显示, BST 纳米粉体颗粒尺寸大约为 100 nm, 当 pH 值为 4 时 BST 纳米颗粒开始通过相互连接形成纳米网状结构。经光催化降解罗丹明 B 研究发现, 在 pH 值为 4 条件下制备的纳米 BST 粉体表现出更高的光催化活性。这可能是因为在 pH 值为 4 时纳米网状结构的 BST 形成提高了光生载流子的迁移率, 从而提高了纳米 BST 在有机物降解过程中光催化效率。

关 键 词: (Ba, Sr)TiO_3; 网状纳米结构; 光催化; 溶胶–凝胶法

中图分类号: X703 **文献标识码:** A